

Force measurements on rising bubbles

By WOODROW L. SHEW, SEBASTIEN PONCET†
AND JEAN-FRANÇOIS PINTON

Laboratoire de Physique, École Normale Supérieure de Lyon, 69007 Lyon, France

(Received 24 May 2006 and in revised form 9 September 2006)

The dynamics of millimetre-sized air bubbles rising through still water are investigated using ultrasound velocimetry combined with high-speed video. From measurements of speed and three-dimensional trajectories we calculate time-resolved precise drag and lift forces on the bubble, which give rise to planar zigzag and three-dimensional spiralling motion. Temporal correlations of forces and the oscillatory bubble motions, particularly the lift force, emphasize the importance of the wake vortices found in previous studies.

1. Background

An understanding of bubble–fluid interactions is important in a broad range of natural, engineering, and medical settings. Air–sea gas transfer, bubble column reactors, oil/natural gas transport, boiling heat transfer, ship hydrodynamics, ink-jet printing and medical ultrasound imaging are just a few examples where the dynamics of bubbles play a role (e.g. Prosperetti 2004; Magnaudet & Eames 2000; Clift, Grace & Weber 1978). We focus on the hydrodynamic forces experienced by a single air bubble rising through still water and the resulting oscillatory bubble trajectories.

Our study includes a range of bubble sizes between 0.87 and 1.2 mm in radius. At the small end of this range the bubble's path is rectilinear. As the bubble size is increased, there is a transition to a planar zigzag path (Mougin & Magnaudet 2002*b*; de Vries, Biesheuvel & van Wijngaarden 2002). A second instability, often preceded by the zigzag, results in a spiralling path (Mougin & Magnaudet 2002*b*; de Vries *et al.* 2002; Brücker 1999; Lunde & Perkins 1997). Larger bubbles may also exhibit oscillatory paths, but typically do not have steady shape and we do not address these motions here.

Leonardo Da Vinci is probably the first scientist to contribute to the significant body of work addressing bubble path instabilities (Prosperetti 2004). Clift *et al.* (1978) review relevant studies prior to about 1978; Magnaudet & Eames (2000) provide a thorough account of more recent work. Our attention will be limited to those works which address path instabilities of bubbles less than 1.25 mm in radius. Saffman (1956), Hartunian & Sears (1957), and Benjamin (1987) attempted to explain features of the path instabilities and bubble shape by analytical means, but experiments and numerics are not in accord with their findings.

Several experimental works have visualized and documented zigzagging and spiralling bubble paths. Aybers & Tapucu (1969*a, b*) used photographic techniques to measure bubble speed, drag coefficients, size, shape, and path. Mercier, Lyrio &

† Present address: Laboratoire de Modélisation et Simulation Numérique en Mécanique et Génie des Procédés, Technopole de Château-Gombert, 38 rue F. Joliot Curie, 13451 Marseille, France.

Forslund (1973) used a stroboscope and several cameras to measure short sections of bubble trajectories. More recently, Wu & Gharib (2002) used a high-speed video three-dimensional imaging system to measure paths and bubble shape. These works advanced qualitative understanding of bubble behaviour and in some cases made average drag coefficient measurements, but did not attempt to explain causal mechanisms or make time-resolved quantitative force measurements.

Other recent studies have investigated path instabilities with special attention paid to the role of the bubble's wake. Lunde & Perkins (1997) used dye to observe the wake of ascending bubbles and solid particles. Brücker (1999) used particle image velocimetry to study the wake of large spiralling bubbles. Mougin & Magnaudet (2002*a, b*) presented numerical observations of the path and wake of a bubble with a rigid ellipsoidal shape. De Vries *et al.* (2002) used schlieren optics techniques to visualize the wakes of zigzagging and spiralling bubbles. Finally, Ellingsen & Risso (2001) used laser Doppler anemometry and cameras to measure the path as well as the flow around the bubble.

These studies have revealed a wake consisting of two long thin parallel vortices aligned with the bubble's path. One vortex rotates clockwise and the other counter-clockwise. For a spiralling bubble the wake vortices are continuously generated, while they are interrupted twice per period of path oscillation for the zigzag. Mougin & Magnaudet (2002*a, b*) observed a nearly identical wake structure in their numerical simulations (see also Mougin 2002). These wake studies reveal that the wake vortices play a critical role in generating hydrodynamic forces on the bubble, which motivates our effort to make quantitative force measurements.

Our approach is to use measurements of three-dimensional bubble trajectories to calculate precise and time-resolved hydrodynamic forces on the bubbles. The aim is to uncover the temporally correlated dynamic behaviour of forces and bubble motion over a large rise distances. Such phenomena are important to model the forces on bubbles accurately.

2. Experimental apparatus and methods

One goal of this work is to obtain measurements of bubbles rising through a large distance, revealing the long-time dynamics of the zigzag and spiral instabilities. The experiments are conducted in an acrylic tank 2 m in height and 30 cm wide with square cross-section as illustrated in figure 1. Bubbles are produced at the bottom of the vessel by pumping air through a stainless steel capillary tube with a 0.30 mm inner diameter (ID) oriented with its open end facing upwards. The air is delivered to the capillary tube through a length of Tygon tubing using a peristaltic pump turned by hand. We always allow at least 3 min. delay between the release of consecutive bubbles to be sure that the water is truly quiescent for each bubble.

The volume of each bubble is measured individually; it is trapped at the end of its rise and then sucked into a thin transparent tube with a syringe with water on either side of the bubble. The length of the air plug in the tube is then used to calculate the bubble volume. In the results that follow, an equivalent radius $R \equiv (3/4\pi \times \text{actual volume})^{1/3}$ is used as a measure of the bubble size. During the ascent, R increases by 6% due to the gradient in hydrostatic pressure. This expansion is accounted for in the calculations of forces. Furthermore, each bubble radius or Reynolds number presented here is properly adjusted for the pressure at the instantaneous height of the bubble. The Reynolds number is defined $Re = 2RU/\nu$, where U is the instantaneous speed of the bubble and ν is the kinematic viscosity of water.

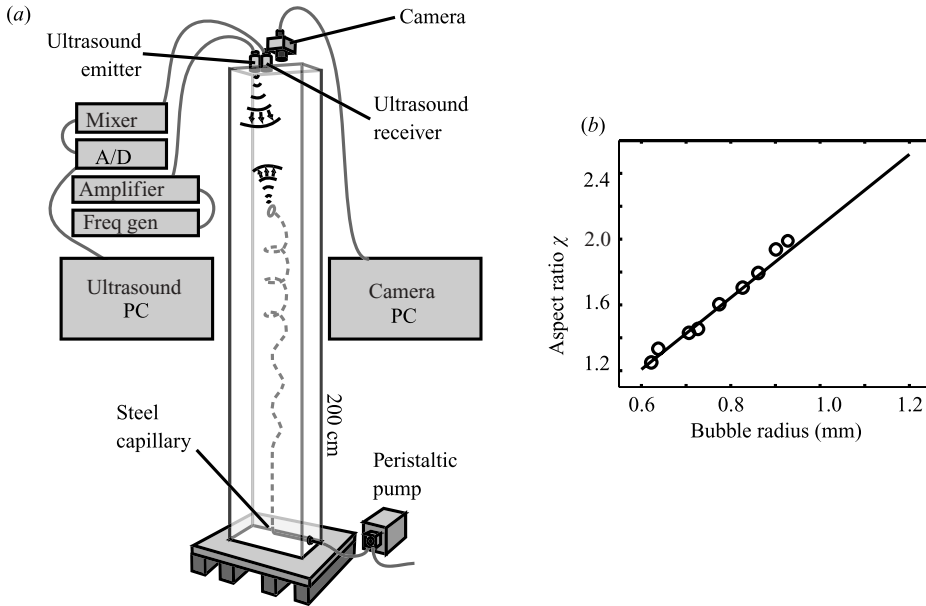


FIGURE 1. (a) Schematic of experimental setup. As the bubble rises its vertical velocity is measured using ultrasound and its horizontal position is obtained with a high-speed video camera. (b) Comparison of Duineveld's (1995) measurements of aspect ratio and the linear model we use to estimate χ .

Some of our force calculations depend on the shape of the bubble. Previous experimental studies show that the bubble is close to an oblate ellipsoid (de Vries *et al.* 2002; Duineveld 1995; Ellingsen & Risso 2001; Wu & Gharib 2002). Since we do not make such measurements, we use the experimental results of Duineveld (1995) (confirmed by Wu & Gharib 2002) to estimate the shape of our bubbles. The aspect ratio χ is the ratio of the length of the semimajor axis to the semiminor axis. The aspect ratio of the bubbles in our size range is approximated well by a linear function of bubble equivalent radius. In figure 1, we show Duineveld's results and the linear fit, $\chi(R) = 2.18R - 0.10$, where R is expressed in mm. This method of estimating χ is supported by the agreement of our measurements with Moore's (1965) drag theory presented in §4.

Before each experiment the vessel and all parts exposed to the water are thoroughly cleaned with methanol, dried, and then rinsed with tap water for 5 min. All data are collected with tap water less than 8 hours old. Temperature is monitored at two different depths for each experiment. The mean temperature is $18.5 \pm 0.25^\circ\text{C}$ and the gradient is always less than $0.009^\circ\text{C cm}^{-1}$. It is known that small bubbles rise more slowly in tap water than in highly purified water due to contamination of the air–water interface with surfactants (e.g. Clift *et al.* 1978; Duineveld 1995). Several observations suggest that our bubbles are not small enough to be greatly influenced by surfactant effects. First, our velocity measurements are consistent with Moore's drag theory and Duineveld's measurements in clean water (see figure 4 in §4). Second, we observe that during the straight rise of a bubble of radius 1.0 mm (at 1 atm), the velocity grows by about 2% over 1.5 m. This result is consistent with the increase in buoyancy and drag due the growth in size as well as aspect ratio during ascent. If surfactant effects were significant, the bubble is likely to slow down as it rises. We note

that for bubbles smaller than about 0.75 mm in radius, our measured rise velocities reveal such a decrease in speed and are lower than those reported by Duineveld. This indicates that, in our tap water, smaller bubbles are strongly influenced by surfactants, while larger bubbles are not. The data presented in this paper are limited to bubbles larger than 0.87 mm.

The trajectory of the bubble is measured using two methods: ultrasound and high-speed video. The vertical component of the bubble velocity is obtained with high precision using a continuous ultrasound technique. We briefly describe this technique here, but for more detail the reader is referred to Mordant & Pinton (2000) and Mordant *et al.* (2005). One piezo-electric ultrasound transducer (Matec 1C-510PE) positioned at the top of the vessel generates continuous 2.8 MHz sound directed towards the bottom. A second piezo transducer (Vermon, custom made) records the sound scattered from the rising bubble. Once digitized, Matlab routines are used to extract the Doppler-shifted frequency of the scattered sound, which is directly proportional to the bubble velocity. To obtain velocity as a function of time, the frequency is extracted using a numerical approximated maximum likelihood scheme coupled with a generalized Kalman filter. The absolute accuracy of our velocity measurements (2%) was verified using a video camera. We measure maximum speeds of our bubbles typically about 36 cm s^{-1} , which is close to other experimental measurements (Duineveld 1995; Aybers & Tapucu 1969*b*; Wu & Gharib 2002). The relative accuracy of our velocity measurements is more precise, typically $\pm 1 \text{ mm s}^{-1}$, or about 0.2% accuracy. Furthermore, the sampling frequency is several kHz. With a 2 m field of observation, this level of accuracy is not feasible with cameras or other optical methods. Another advantage is that the ultrasound technique is potentially useful in opaque fluids.

A high-speed video camera (Photron Fast Cam Ultima 1024, 125 frames/sec, 512×512 pixels) is positioned above the vessel close to the ultrasound receiving array so that it records the lateral movement of the bubble. The bubble position is extracted from movies using Matlab image processing routines. The accuracy of the position measurements is about 3% or $\pm 0.1 \text{ mm}$ with 8 ms time resolution. The horizontal position data are differentiated to obtain the horizontal velocity with about 6% or $\pm 6 \text{ mm s}^{-1}$ precision.

From the vertical speed and horizontal position data we can reconstruct the entire three-dimensional trajectory for each bubble as demonstrated in figure 2, for a bubble 1.12 mm in radius at atmospheric pressure. This example demonstrates the three different types of behaviour exhibited by the bubbles in the size range of our investigation. Just after the bubble is generated it accelerates quickly to its terminal speed. It rises for a short time in a nearly straight path. For a large enough bubble, the rectilinear rise soon becomes unstable to a zigzag motion. These oscillations are confined to a vertical plane (y, z -plane in figure 2). The path then evolves into a spiral. A smooth transition occurs from zigzag to a precessing elliptical spiral, and finally to a circular spiral. This transition is shown in figure 3(*a*), where the trajectory is projected onto a horizontal plane.

3. Forces on bubbles

The equations of motion for a rigid body moving through a fluid at rest were established in the context of potential flow theory more than a century ago by Kirchhoff (Lamb 1945, chap. VI). Like other analytical approaches to understanding bubble dynamics, potential flow theory describes the gross features, but regions of the flow with vorticity must be accounted for in order to make precise predictions. Kirchhoff's equations have been generalized to the case of viscous, rotational flow and bodies

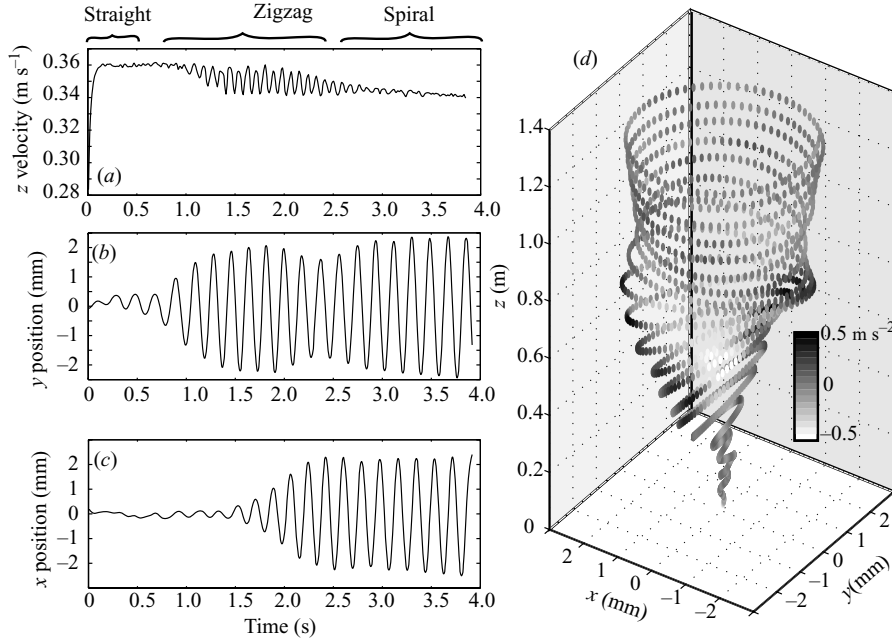


FIGURE 2. Example trajectory of a 1.12 mm radius bubble (at 1 atm). (a) Vertical component of velocity as measured with ultrasound technique, (b) y position from camera data, (c) x position from camera data, and (d) three-dimensional reconstruction of full trajectory with greyscale indicating magnitude of acceleration. The bubble begins rising straight, followed by zigzag motion in the (y, z) -plane with oscillating velocity, followed by a three-dimensional spiral motion with steady velocity.

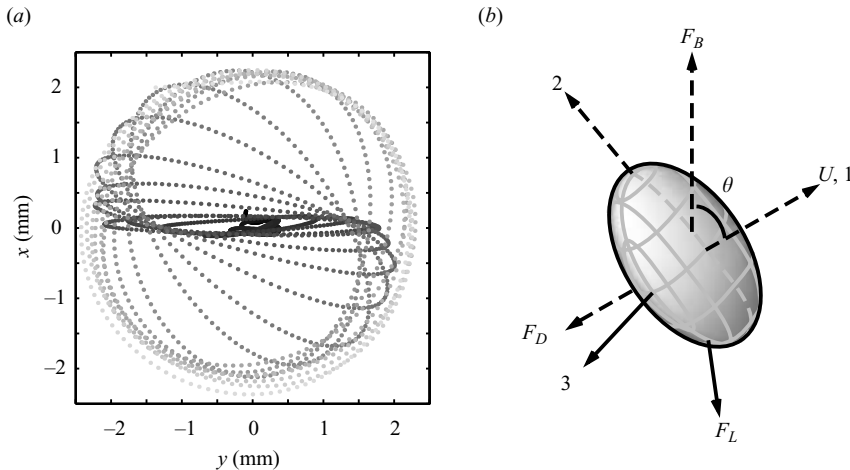


FIGURE 3. (a) Projection of a bubble trajectory onto a horizontal plane during the transition from zigzag to spiral (see also x and y data in figures 2(b) and 2c). Greyscale indicates time: black at $t = 0$ and light grey at $t = 4$ s. The bubble radius is 1.12 mm at 1 atm. (b) Diagram of the coordinate system, velocity U , pitch angle θ , and external forces (F_B , F_D , F_L) present for a spiralling bubble. The dashed lines lie in the 1–2 plane.

with free slip boundaries (Howe 1995 also addressed no-slip boundaries) and, more recently, used in numerical work (Mougin & Magnaudet 2002*a, b*) to investigate the behaviour of freely rising bubbles with a fixed shape. The numerical work revealed the

same zigzagging and spiralling paths as we and others have observed experimentally as well as quantitative agreement with path oscillation amplitudes and frequencies. These results strongly suggest that shape changes to the bubble do not play a critical role in the dynamics. This work as well as experimental observations (Ellingsen & Risso 2001) of steady bubble shapes for the size range we study lead us to assume that bubble shape is fixed and to use the generalized Kirchhoff equations. (We note that de Vries 2001 reports that zigzagging bubbles may have a slightly oscillating shape. We will address the consequences of this for our measurement uncertainty in §4.)

The Kirchhoff equations govern the six degrees of freedom necessary to completely specify the angular velocity $\boldsymbol{\Omega}$ and the linear velocity \boldsymbol{U} of a body:

$$\mathbb{A}_{ij} \frac{dU_j}{dt} + \epsilon_{ijk} \Omega_j \mathbb{A}_{kl} U_l = F_i + F_{Bi}, \quad (3.1)$$

$$\mathbb{D}_{ij} \frac{d\Omega_j}{dt} + \epsilon_{ijk} \Omega_j \mathbb{D}_{kl} \Omega_l + \epsilon_{ijk} U_j \mathbb{A}_{kl} U_l = \Gamma_i, \quad (3.2)$$

where \mathbb{A} and \mathbb{D} are the added mass and added rotational inertia tensors and ϵ is the permutation tensor. The hydrodynamic forces and torques experienced by the bubble are F_i and Γ_i , and F_B , not F_B is the buoyancy force. The dynamic quantities in (3.1) and (3.2) are evaluated in the lab frame (Galilean) and projected onto a coordinate system which rotates with the bubble, precisely defined as follows. The 1-direction is always parallel to the velocity vector of the bubble. The 2-direction is at a right angle to the 1-direction. It is defined such that the 1–2 plane is vertical and the 2-direction evolves continuously. Finally, the 3-direction is orthogonal to the 1- and 2-directions and, hence, is always purely horizontal. This coordinate system is right-handed and Cartesian as illustrated in figure 3(b).

For an air bubble rising through still water, the hydrodynamic forces \boldsymbol{F} , by assumption, include only drag and lift. Drag represents those forces parallel to the bubble trajectory which cannot be accounted for by F_{B1} and lift represents those forces acting perpendicular to the bubble trajectory which cannot be accounted for by F_{B2} . Generally, $\boldsymbol{F} = (F_D + F_{B1}, F_{L2} + F_{B2}, F_{L3})$. History forces are not dealt with explicitly, but are implicit in the time dynamics of drag and lift. For the size range of bubbles we study, it has been observed in experiments and numerics that the short axis of the ellipsoidal bubble is nearly aligned with the bubble velocity vector at all times (Ellingsen & Risso 2001; de Vries *et al.* 2002; Mougin & Magnaudet 2002*b*). Using the approximation that they are perfectly aligned determines the rotational degrees of freedom, which eliminates the need to consider (3.2) and gives

$$\Omega_1 = \frac{d\phi}{dt} \cos \theta, \quad \Omega_2 = \frac{d\phi}{dt} \sin \theta, \quad \Omega_3 = -\frac{d\theta}{dt}, \quad (3.3)$$

where θ is the pitch angle of the path and ϕ is the azimuthal angle between a fixed horizontal line and the horizontal projection of the 1-direction. With the above-defined assumptions and coordinate system, $\boldsymbol{U} = (U, 0, 0)$ and \mathbb{A} is time independent and diagonal. Equation (3.1) then reduces to

$$\mathbb{A}_{11} \frac{dU}{dt} = F_D + F_{B1}, \quad \Omega_3 \mathbb{A}_{11} U = F_{L2} + F_{B2}, \quad -\Omega_2 \mathbb{A}_{11} U = F_{L3}. \quad (3.4)$$

In the above notation, $F_{B1} = \rho V g \cos \theta$ and $F_{B2} = \rho V g \sin \theta$, where $\rho = \rho_f - \rho_g \approx \rho_f$ is the density difference between the fluid and the gas, V is the volume of the bubble, and g is acceleration due to gravity. \mathbb{A}_{11} ranges from 1.18 to 1.37 for our range of aspect ratios $2.1 < \chi < 2.4$ (see e.g. art. 114 in Lamb 1945). Using our measurements of vertical velocity, horizontal position and bubble size, it is a matter of geometry to

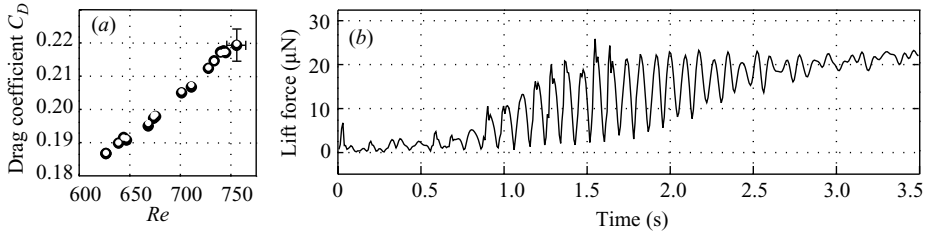


FIGURE 4. (a) Comparison of our drag coefficient measurements (black circles, representative error bar shown) during the rectilinear part of the bubble trajectories to predictions of Moore's theory (white circles). (b) The total magnitude of lift $|F_L| = \sqrt{F_{L2}^2 + F_{L3}^2}$ as measured during the trajectory shown in figure 2. The bubble radius is 1.12 mm at 1 atm. The measurement uncertainty is about $\pm 4 \mu\text{N}$.

calculate U , θ , and $d\phi/dt$: $\theta = \arccos(u_z/U)$ and $d\phi/dt = (u_x \dot{u}_y - \dot{u}_x u_y)/u_h^2$, where the total horizontal component of velocity is u_h , the over-dot signifies a time derivative, and (x, y, z) are as defined in figure 2(d). Note that for planar motion (zigzag) the sign of θ must be assigned using a post-processing algorithm. The drag and lift forces are the only remaining unknowns and may be calculated from (3.4).

4. Experimental observations

We first discuss several observations of the initial moments of the bubble's ascent to the point where the trajectory becomes unstable. Once the bubble has attained terminal velocity it typically rises for a short period in a straight trajectory before beginning to zigzag. In figure 4(a), we compare our measurements of the drag coefficient $C_D(\chi, Re)$ during the constant-speed rectilinear portion of the trajectory to Moore's (1965) theory. The excellent agreement with Moore's theory and, hence, other experiments provides additional validation of our measurement techniques and methods of analysis. Note that Moore's prediction of $\chi(R)$ does not agree with experiments (Duineveld 1995) and therefore we obtain the aspect ratio empirically as described in § 2.

We observe that the height above the release point at which a bubble's path becomes unstable varies significantly with bubble size. Small bubbles can rise straight for nearly 2 m before becoming unstable, while larger bubbles may become unstable even before reaching terminal velocity. For those bubbles whose path becomes unstable some time after reaching terminal velocity, we determine that the critical radius at the onset of oscillations is 0.97 mm. Using the approximation shown in figure 1(b), this corresponds to a critical aspect ratio of 2.02.

As demonstrated in figure 5(a) the zigzag path is a smooth sinusoid confined to one vertical plane. One important observation is that the speed of the bubble oscillates during the zigzag motion. The speed oscillations are twice the frequency of the path oscillations. The drag also oscillates at twice the path oscillation frequency, while the lift has the same frequency as the path oscillation.

First, we discuss the magnitude of the lift force, which is shown for an entire bubble trajectory in figure 4(b). Focusing on the 2-component of lift (see figure 5(a), we observe that the magnitude $|F_{L2}|$ reaches a maximum 25–30 ms after the maximum in bubble speed. Similarly $|F_{L2}|$ is zero about 25–30 ms after the minimum bubble speed, suggesting the importance of a dynamic response time $\tau \approx 25$ ms. Note that $|F_{L2}|$ is not zero at the point of inflection of the path as has been suggested by other authors, but also about 25 ms later. At the inflection point, path curvature is zero, but

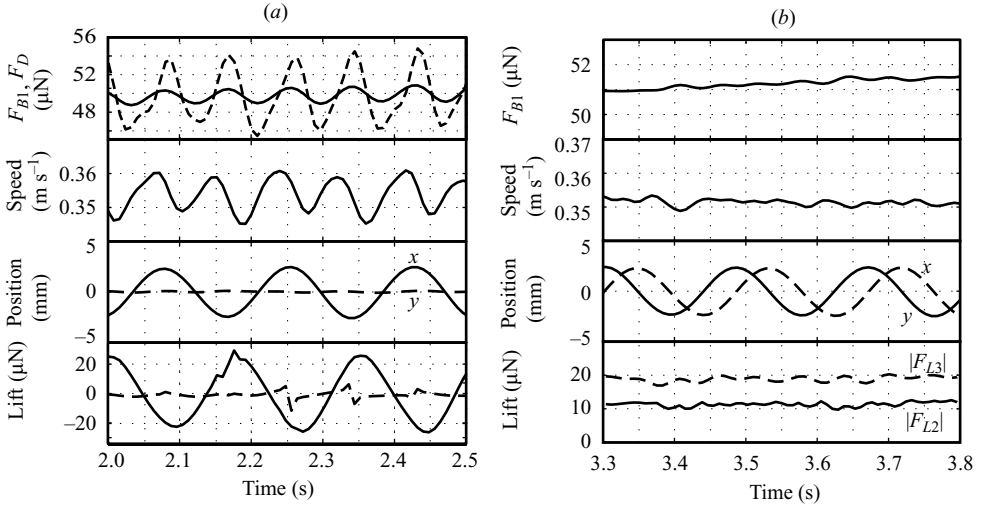


FIGURE 5. The buoyancy component tangential to the path F_{B1} (solid line), drag F_D (dashed line), bubble velocity, horizontal position (x and y), and lift force magnitudes (solid line: $|F_{L2}|$ and dashed line: $|F_{L3}|$) as measured during a zigzagging trajectory (a) and a spiralling trajectory (b). The bubble radius is 1.12 mm at 1 atm. The measurement uncertainties are $\pm 0.5 \mu\text{N}$ for F_{B1} and F_D , $\pm 7 \text{ mm s}^{-1}$ for speed, $\pm 0.2 \text{ mm}$ for position, and $\pm 4 \mu\text{N}$ for lift forces.

the lift must remain non-zero to balance F_{B2} . The buoyant force begins to accelerate the bubble again just before and after the instant when $F_{L2} = 0$. Some researchers have proposed that the lift arises from the wake vortices discussed in §1 and that the wake vortices develop when vorticity production on the bubble surface is large enough (de Vries *et al.* 2002; Mougin & Magnaudet 2002b; Lunde & Perkins 1997). The time dynamics and our lift measurements are consistent with this. In this context our measured lag between velocity and lift fluctuations suggests that wake vortex growth may be hysteretic since vorticity production is proportional to bubble speed.

We turn now to drag. We find that the oscillations in F_{B1} alone cannot account for the oscillations in speed of the zigzagging bubble. Therefore F_D must oscillate as well. The oscillations in F_D are not as one might expect from standard drag formulas. That is, increasing speed does not coincide with an increase in the magnitude $|F_D|$. Rather, increasing $|F_D|$ is apparently tied to increasing $|F_{L2}|$ as is evident in figure 5(a). Thus, the repeating decrease in bubble speed during the zigzag must be attributed to both a reduction in F_{B1} and an increase in $|F_D|$.

As mentioned in §3, our measurements depend on the assumption of steady bubble shape. While Ellingsen & Risso (2001) report steady shape, de Vries (2001) suggests that the shape of zigzagging bubbles oscillates slightly. Based on de Vries' schlieren photos, we estimate an upper limit for changes in χ to be about 10%. Such a variation would result in 5% change in the magnitude of F_{L2} and no more than 1 ms change in time dynamics. Therefore, the above discussion would be largely unaffected by such shape changes. For spiralling bubbles de Vries agrees that the shape is steady.

We now turn to the dynamics of spiralling bubble motion. The transition to spiral motion is remarkable in several ways. First, we observe that every zigzagging path eventually becomes a spiral. The spiral may be clockwise or counterclockwise. Bubbles may zigzag for as many as 15 and as few as 2 cycles before transitioning to the spiral. The transition is not abrupt, generally developing gradually over several periods of motion with non-trivial dynamical changes in the direction of the lift force

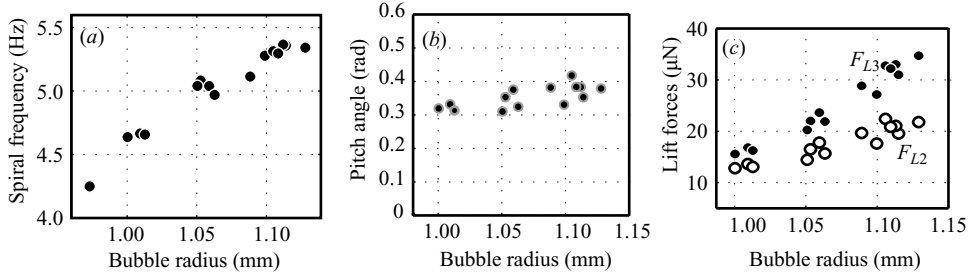


FIGURE 6. (a) The frequency of spiralling motion for a range of bubble sizes. The measurement is precise to within 2%. (b) The average pitch angle during spiral motion. (c) Comparison of F_{L2} (open circles) and F_{L3} (solid circles) for spiralling bubbles. The measurement uncertainty is $\pm 2 \mu\text{N}$.

components. Furthermore, the transition does not behave systematically with bubble size. The frequency of path oscillations remains unchanged compared to the zigzag. This is apparent in the horizontal position data shown in figure 2. The frequency increases as bubble size is increased as shown in figure 6(a). From (3.3) and (3.4) we can derive a formula for the spiral frequency, which is equivalent to the magnitude of $d\phi/dt$. We obtain $d\phi/dt = F_{L3}/\mathbf{A}_{11}U \sin \theta$. Excellent agreement with the measured spiral frequencies (e.g. 5.1 Hz for a 1.05 mm radius bubble) provides a consistency check and support for our force calculation methods.

The most striking change when the bubble stops zigzagging and begins to spiral is that all the forces, the bubble speed, and the pitch angle become steady. Figure 5(b) shows time series of several features of a spiralling bubble. The top frame presents the component of buoyancy F_{B1} . Since the speed of the bubble is constant during the spiral, F_{B1} is equal in magnitude to the drag on the bubble. We observe that the magnitude of this drag is nearly equal to that predicted for a bubble at the same speed using Moore's formula. This is probably coincidental since Moore's theory is based on a different wake flow structure and our drag measurements during the zigzag are clearly not described well by Moore's theory. The component of lift F_{L2} is constant in time, balancing F_{B2} . We observe that F_{L3} is typically about twice as large as F_{L2} , and also constant in time. This is apparent in figure 5(b) and is quantified for a range of bubble sizes in figure 6(c). The average value of pitch angle during spiral motion is typically around 0.35 rad as shown in figure 6(b).

5. Conclusions

Using an ultrasound device and a video camera, we make precise measurements of speed and three-dimensional trajectories of millimetre-sized air bubbles rising through 2 m of still water. We use these measurements to calculate drag and lift forces acting on the bubble. We observe that for the rectilinear portion of bubble trajectories the measured drag matches Moore's prediction. We measure $10 \mu\text{N}$ oscillations in drag, which cannot be explained by Moore's theory, and $20\text{--}40 \mu\text{N}$ oscillations in lift for zigzagging bubbles. Lift fluctuations correlate with velocity fluctuations with a 25 ms delay. The direction of the lift force exhibits non-trivial dynamics during the transition from zigzag to spiral, finally reaching steady values, $10\text{--}40 \mu\text{N}$ in magnitude (buoyancy is typically $50\text{--}60 \mu\text{N}$). Our force measurements are consistent with the idea that wake vortices dominate the dynamics of path instabilities. The force measurement technique developed here could be applied in future experiments with different liquids and gases,

accompanied by bubble shape measurements to elucidate surface tension and other fluid property effects on the zigzag and spiral trajectories.

We thank Jacques Magnaudet for helpful advice on the Kirchhoff equations. This work was funded by École Normale Supérieure, Centre National de la Recherche Scientifique, and Région Rhône-Alpes, Emergence Contract 0501551301.

REFERENCES

- AYBERS, N. M. & TAPUCU, A. 1969a The motion of gas bubbles rising through stagnant liquid. *Wärme- und Stoffübertragung* **2**, 118.
- AYBERS, N. M. & TAPUCU, A. 1969b Studies on the drag and shape of gas bubbles rising through stagnant liquid. *Wärme- und Stoffübertragung* **2**, 171.
- BATCHELOR, G. K. 1967 *An Introduction to Fluid Dynamics*. Cambridge University Press.
- BENJAMIN, T. B. 1987 Hamiltonian theory for motions of bubbles in an infinite liquid. *J Fluid Mech* **181**, 349.
- BRÜCKER, C. 1999 Structure and dynamics of the wake of bubbles and its relevance for bubble interaction. *Phys Fluids* **11**, 1781.
- CLIFT, R., GRACE, J. R. & WEBER, M. E. 1978 *Bubbles, Drops, and Particles*. Academic.
- DUINEVELD, P. C. 1995 The rise velocity and shape of bubbles in pure water at high Reynolds number. *J Fluid Mech* **292**, 325.
- ELLINGSEN, K. & RISSO, F. 2001 On the rise of an ellipsoidal bubble in water: oscillatory paths and liquid-induced velocity. *J Fluid Mech* **440**, 235.
- HARTUNIAN, R. A. & SEARS, W. R. 1957 On the instability of small gas bubbles moving uniformly in various liquids. *J Fluid Mech* **3**, 27.
- HOWE, M. S. 1995 On the force and moment on a body in an incompressible fluid, with application to rigid bodies and bubbles at low and high Reynolds numbers. *Q. J. Mech. Appl. Maths* **48**, 401.
- LAMB, H. 1945 *Hydrodynamics*, 6th Edn. Dover.
- LUNDE, K. & PERKINS, R. J. 1997 Observations on wakes behind spheroidal bubbles and particles. *ASME FED Summer Meeting, Vancouver, Canada*, Paper FEDSM'97-3530.
- MAGNAUDET, J. & EAMES, I. 2000 The motion of high-Reynolds-number bubbles in inhomogeneous flows. *Annu. Rev. Fluid Mech.* **32**, 659.
- MERCIER, J., LYRIO, A. & FORSLUND, R. 1973 Three dimensional study of the nonrectilinear trajectory of air bubbles rising in water. *J. Appl. Mech.* **40**, 650.
- MOORE, D. W. 1965 The velocity of rise of distorted gas bubbles in a liquid of small viscosity. *J. Fluid Mech.* **23**, 749.
- MORDANT, N., METZ, P., MICHEL, O. & PINTON, J.-F. 2005 An acoustic technique for Lagrangian velocity measurements. *Rev. Sci. Instrum.* **76**, 025105.
- MORDANT, N. & PINTON, J.-F. 2000 Velocity measurements of a settling sphere. *Eur. Phys. J. B* **18**, 343.
- MOUGIN, G. 2002 Interactions entre la dynamique d'une bulle et les instabilités de son sillage. PhD Dissertation, Institute National Polytechnique de Toulouse, France.
- MOUGIN, G. & MAGNAUDET, J. 2002a The generalized Kirchhoff equations and their application to the interaction between a rigid body and an arbitrary time-dependent viscous flow. *Intl J. Multiphase Flow* **28**, 1837.
- MOUGIN, G. & MAGNAUDET, J. 2002b Path instability of a rising bubble. *Phys. Rev. Lett.* **88**, 014502.
- PROSPERETTI, A. 2004 Bubbles. *Phys. Fluids* **16**, 1852.
- SAFFMAN, P. G. 1956 On the rise of small air bubbles in water. *J. Fluid Mech.* **1**, 249.
- DE VRIES, A. W. G. 2001 Path and wake of a rising bubble. PhD dissertation, University of Twente, Netherlands.
- DE VRIES, A. W. G., BIESHEUVEL, A. & VAN WIJNGAARDEN, L. 2002 Notes on the path and wake of a gass bubble rising in pure water. *Intl J. Multiphase Flow* **28**, 1823.
- WU, M. & GHARIB, M. 2002 Experimental studies on the shape and path of small air bubbles rising in clean water. *Phys. Fluids* **14**, L49.